Phase-contrast imaging using a scanning-double-grating configuration

Ya. I. Nesterets* **and S. W. Wilkins**

CSIRO Materials Science and Engineering, PB33, Clayton South, VIC 3169, Australia
**Corresponding author: Yakov.Nesterets@csiro.au*

Abstract: A new double-grating-based phase-contrast imaging technique is described. This technique differs from the conventional double-grating imaging method by the image acquisition strategy. The novelty of the proposed method is in lateral scanning of both gratings simultaneously while an image is collected. The collected image is not contaminated by a Moiré pattern and can be recorded even by using a high-spatial-resolution integrating detector (e.g. X-ray film), thus facilitating improved resolution and/or contrast in the image. A detailed theoretical analysis of image formation in the scanning-double-grating method is carried out within the rigorous wave-optical formalism. The transfer function for the scanning-double-grating imaging system is derived. An approximate geometrical-optics solution for the image intensity distribution is derived from the exact wave-optical formula using the stationary-phase approach. Based on the present formalism, the effects of finite source size on the preferred operating conditions and of polychromaticity on the image contrast and resolution are investigated.

OCIS codes: (110.7440) X-ray imaging; (110.6760) Talbot and self-imaging effects; (110.4850) Optical transfer functions; (110.4980) Partial coherence in imaging.

References and links

1. U. Bonse and M. Hart, "An x-ray interferometer," Appl. Phys. Lett. **6**, 155-156 (1965).
2. M. Ando and S. Hosoya, "An attempt at x-ray phase-contrast microscopy," in Proc. 6th Intern. Conf. On X-ray Optics and Microanalysis, G. Shinoda, K. Kohra and T. Ichinokawa Eds. (Univ. of Tokyo Press, Tokyo, 1972) pp. 63-68.
3. A. Momose, "Demonstration of phase-contrast X-ray computed tomography using an X-ray interferometer," Nucl. Instrum. Methods A **352**, 622-628 (1995).
4. K. Goetz, M. P. Kalashnikov, Yu. A. Mikhailov, G. V. Sklizkov, S. I. Fedotov, E. Foerster and P. Zaumseil, "Measurements of the parameters of shell targets for laser thermonuclear fusion using an x-ray schlieren method," Sov. J. Quantum Electron. **9**, 607-610 (1979).
5. V. A. Somenkov, A. K. Tkalich and S. Sh. Shil'shtein, "Refraction contrast in x-ray introscopy," Sov. Phys. Tech. Phys. **36**, 1309-1311 (1991).
6. V. N. Ingal and E. A. Beliaevskaya, "X-ray plane-wave topography observation of the phase contrast from a non-crystalline object," J. Phys. D: Appl. Phys. **28**, 2314-2317 (1995).
7. T. J. Davis, D. Gao, T. E. Gureyev, A. W. Stevenson and S. W. Wilkins, "Phase-contrast imaging of weakly absorbing materials using hard X-rays," Nature **373**, 595-598 (1995).
8. J. F. Clauser, "Ultrahigh resolution interferometric X-ray imaging," US patent No. 5,812,629 (1998).
9. C. David, B. Nöhammer, H. H. Solak and E. Ziegler, "Differential x-ray phase contrast imaging using a shearing interferometer," Appl. Phys. Lett. **81**, 3287-3289 (2002).
10. A. Momose, S. Kawamoto, I. Koyama, Y. Hamaishi, K. Takai and Y. Suzuki, "Demonstration of X-Ray Talbot Interferometry," Jpn. J. Appl. Phys. **42**, L866-L868 (2003).
11. C. David, "Apparatus and method to obtain phase contrast x-ray images," Europ. patent No. EP 1,447,046-A1; Internat. publ. No. WO 2004/071298-A1; Aust. patent No. AU 2003/275964-A1 (2004).
12. T. Weitkamp, B. Nöhammer, A. Diaz, C. David and E. Ziegler, "X-ray wavefront analysis and optics characterization with a grating interferometer," Appl. Phys. Lett. **86**, 054101 (2005).
13. T. Weitkamp, A. Diaz, C. David, F. Pfeiffer, M. Stampanoni, P. Cloetens and E. Ziegler, "X-ray phase imaging with a grating interferometer," Opt. Express **13**, 6295-6304 (2005).

#92070 - $15.00 USD Received 24 Jan 2008; revised 21 Feb 2008; accepted 21 Feb 2008; published 11 Apr 2008

14. C. David, T. Weitkamp and F. Pfeiffer, "Interferometer for quantitative phase contrast imaging and tomography with an incoherent polychromatic x-ray source," Europ. patent No. EP 1,731,099-A1; Internat. publ. No. WO 2006/131235-A1 (2006).
15. F. Pfeiffer, T. Weitkamp, O. Bunk and C. David, "Phase retrieval and differential phase-contrast imaging with low-brilliance X-ray sources," Nature Physics **2**, 258-261 (2006).
16. T. Weitkamp, C. David, C. Kottler, O. Bunk and F. Pfeiffer, "Tomography with grating interferometers at low-brilliance sources," Proc. SPIE **6318**, 63180S (2006).
17. A. Momose, W. Yashiro, Y. Takeda, Y. Suzuki and T. Hattori, "Phase Tomography by X-ray Talbot Interferometry for Biological Imaging," Jpn. J. Appl. Phys. **45**, 5254-5262 (2006).
18. Y. Takeda, W. Yashiro, Y. Suzuki, S. Aoki, T. Hattori and A. Momose, "X-Ray Phase Imaging with Single Phase Grating," Jpn. J. Appl. Phys. **46**, L89-L91 (2007).
19. A. Snigirev, I. Snigireva, V. Kohn, S. Kuznetsov and I. Schelokov, "On the possibilities of x-ray phase contrast microimaging by coherent high-energy synchrotron radiation," Rev. Sci. Instrum. **66**, 5486-5492 (1995).
20. S. W. Wilkins, T. E. Gureyev, D. Gao, A. Pogany and A. W. Stevenson, "Phase-contrast imaging using polychromatic hard X-rays," Nature **384**, 335-338 (1996).
21. P. Cloetens, R. Barrett, J. Baruchel, J.-P. Guigay and M. Schlenker, "Phase objects in synchrotron radiation hard x-ray imaging," J. Phys. D: Appl. Phys. **29**, 133-146 (1996).
22. T. E. Gureyev, Ya. I. Nesterets, D. M. Paganin, A. Pogany and S. W. Wilkins, "Linear algorithms for phase retrieval in the Fresnel region. 2. Partially coherent illumination," Opt. Commun. **259**, 569-580 (2006).
23. L. Mandel and E. Wolf, *Optical Coherence and Quantum Optics* (Cambridge University Press, Cambridge, 1995).
24. Ya. I. Nesterets, P. Coan, T. E. Gureyev, A. Bravin, P. Cloetens and S. W. Wilkins, "On qualitative and quantitative analysis in analyser-based imaging," Acta Cryst. A **62**, 296-308 (2006).
25. M. V. Fedoryuk, "The stationary phase method and pseudodifferential operators," Russ. Math. Surveys **26**, 65-115 (1971).

1. Introduction

The conventional and long-standing method for X-ray imaging (radiography) is based on absorption and dates back to the pioneering work of Röntgen who discovered X-rays in 1895. More recently, other methods for X-ray imaging have been developed involving phase contrast. These methods are sensitive to the real part of the complex refractive index describing the interaction between electromagnetic radiation and matter. They also notably depend on the use of wave optics for their proper description cf conventional treatments of radiography that are based on simple geometrical optics.

The existing methods for direct X-ray phase-contrast imaging can be classified in terms of their sensitivity to the phase variations in the detected object wave as follows:

1. X-ray interferometry [1-3] which is sensitive to the phase itself but modulo 2π;
2. Differential phase-contrast methods, including analyzer-based imaging (ABI) [4-7] and grating-based imaging [8-18], which are sensitive to the phase derivative in a certain direction or to the phase gradient;
3. Near-field propagation-based imaging (PBI) [19-21] where the image contrast is proportional to the two-dimensional (2D) Laplacian of the phase.

Some of the salient advantages and disadvantages of the above methods are briefly summarized in Table 1 below.

The original grating-based imaging (GBI) method, see Fig. 1, uses two gratings (the first grating is usually phase type and the second grating is amplitude type) with the grating lines parallel to the y-axis and the positions of which along the *x*-axis are fixed for each collected image. The relative offset of the second grating with respect to the first one, along the *x*-axis, may be changed in order to obtain different types of contrast in the images (e.g. dark-field and differential-contrast images) as well as for collecting multiple images (phase-stepping technique) and subsequent processing of them in order to extract a phase derivative distribution (see, for example, [17,18]).

We propose here a new modality for grating-based imaging that utilizes the same basic setup. The only difference is that both gratings are scanned simultaneously (keeping the relative offset along the *x*-axis fixed for any given scan but adjustable) along the *x*-axis while

#92070 - $15.00 USD Received 24 Jan 2008; revised 21 Feb 2008; accepted 21 Feb 2008; published 11 Apr 2008

collecting an image. The resultant image has potentially better resolution and contrast (if used with a high resolution detector) compared to the standard double-grating imaging modality.

Table 1. Some characteristics of the direct phase-contrast imaging techniques

Advantages	Disadvantages
X-ray interferometry	
1. High sensitivity to the phase shift (can achieve sensitivity in $\Delta\rho/\rho$ of order 10^{-9}).	1. Typically requires quasi-monochromatic radiation ($\Delta\lambda/\lambda\sim10^{-4}$). 2. Needs precise alignment of the crystals and is susceptible to mechanical and thermal instabilities. 3. Interferograms are difficult to interpret and typically require more than one interferogram to be recorded for a given sample because of modulo 2π ambiguity. 4. Needs image processing for visualization of the phase. 5. Severe practical difficulties for treating large objects.
Analyzer-based imaging (ABI)	
1. High sensitivity to the phase gradient. 2. Images are easy to interpret (no need for processing). 3. Dark-field imaging is possible.	1. Typically uses quasi-monochromatic radiation ($\Delta\lambda/\lambda\sim10^{-4}$). 2. Usually sensitive to only one component of the phase gradient leading to possible ambiguities in phase estimation. 3. Needs a perfect analyzer crystal that needs to be very precisely controlled in angle. 4. Bent-crystal optics may help to overcome some limitations, but lead to other complications. 5. Spatial resolution is limited by extinction length of analyzer and can be improved by using asymmetric reflections (grazing incidence) for the analyzer crystal.
Grating-based imaging (GBI)	
1. High sensitivity to the phase gradient. 2. Images are easy to interpret (when using two gratings). 3. Moderate polychromaticity is allowed ($\Delta\lambda/\lambda\sim0.1$ **[17]** or even $\Delta\lambda/\lambda\sim1$ **[13]**). 4. Dark-field imaging is possible.	1. Sensitive to only one component of the phase gradient. 2. Needs precise alignment of the gratings at a significant separation distance (in two grating modality). 3. Needs gratings with small period (of the order of several microns) and high aspect ratio. 4. Resolution is decreased intentionally (in two grating modality) or needs collecting several images using a high-resolution detector with further processing of data (single grating modality **[18]**) and may involve ambiguities in phase determination. 5. The need to collect multiple images in a short-time frame for dynamic imaging studies places severe design constraints on suitable detectors. 6. Spatial resolution limited by grating period.
Propagation-based imaging (PBI)	
1. High sensitivity to abrupt phase changes (edge enhancement). 2. Significant polychromaticity is allowed ($\Delta\lambda/\lambda\sim1$ **[20]**). 3. Two-dimensional. 4. Easy to interpret. 5. The simplest setup (no need for optical elements between an object and detector). 6. Can be used to achieve very high spatial resolution.	1. Needs high transverse coherence (distant or small source). 2. Lower contrast compared to other imaging methods.

#92070 - $15.00 USD Received 24 Jan 2008; revised 21 Feb 2008; accepted 21 Feb 2008; published 11 Apr 2008

Moreover, by comparison with the single-grating imaging modality [18], it does not need the acquisition of multiple images and further numerical processing of them (thus even high-resolution X-ray film can be used as the detection medium). There is, however, a strict requirement on the imaging setup in terms of sufficient mechanical stability, namely that both gratings should be scanned along the *x*-axis while keeping their relative motion and orientation fixed to significantly less than a grating period.

The present paper is organized as follows. In section 2.1 we derive a rigorous wave-optical formalism for image formation in the case of an arbitrary scanning double-screen imaging system assuming a monochromatic plane incident wave. In section 2.2, this approach is generalized to the case of partially coherent incident illumination. A geometrical optics approximation to the general solution is derived in section 2.3. The rigorous wave-optical formalism is then applied in section 3 to the scanning-double-grating (SDG) imaging system. Effects of the source size and polychromaticity on the SDG images are analyzed in section 4. The main conclusions are presented in section 5.

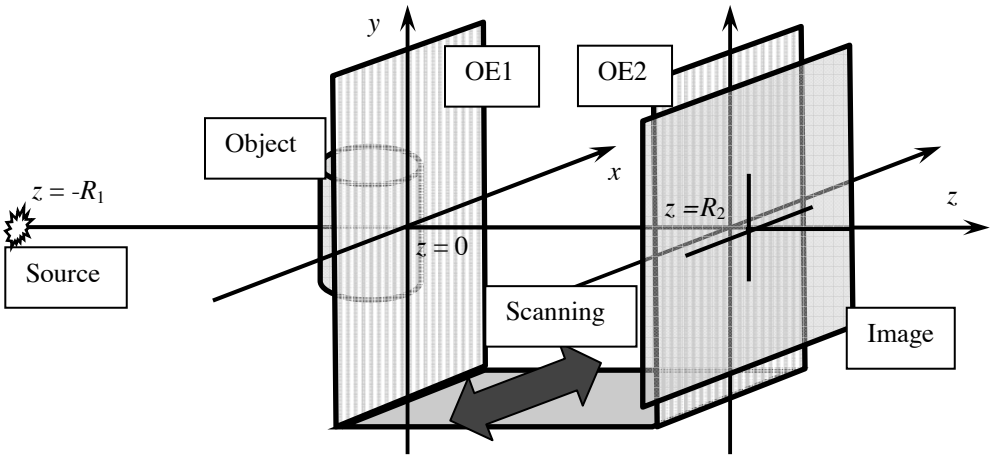

Fig. 1. Schematic representation of the scanning double-screen imaging system.

2. Scanning double-screen image formation

2.1. Monochromatic plane incident wave

Let us consider the imaging setup presented in Fig. 1. Here *OE*1 and *OE*2 are the first and the second optical elements (e.g. slits or gratings) respectively, separated along the *z*-axis by a distance R_2. Both optical elements are characterized by their complex transmission functions, $t_1(x)$ and $t_2(x)$, which are here assumed to depend only on the *x*-coordinate. We restrict our consideration to the case where the first optical element is located immediately after an object, in the exit plane of the object (the object plane, for brevity), and the distance between the second optical element and the detector is negligibly small. Designating $q(x, y)$ as the complex transmission function of the object and assuming that a monochromatic plane wave (i.e. $R_1 >> R_2$) of unit intensity and wavelength λ is incident onto the object, the complex amplitude of the wave immediately after the *OE*1 is written as follows,

$$E_{OE1}(x, y; x_0) = q(x, y)t_1(x - x_1), \tag{1}$$

where x_1 is a position of the *OE*1 along the *x*-axis. The corresponding wave amplitude in the detector plane is then

$$E_{det}(x, y; x_1, \Delta x) = \left(E_{OE1} * P_{R_2}\right)(x, y; x_1)\, t_2(x - x_1 - \Delta x), \tag{2}$$

#92070 - $15.00 USD Received 24 Jan 2008; revised 21 Feb 2008; accepted 21 Feb 2008; published 11 Apr 2008

where $x_1 + \Delta x$ is a position of $OE2$ along the x-axis ($OE2$ is off-set a distance Δx with respect to $OE1$), $P_z(x,y) = P_z(x)P_z(y) \equiv (i\lambda z)^{-1}\exp[i\pi(x^2+y^2)/(\lambda z)]$ is a paraxial approximation for the two-dimensional (2D) free-space propagator at a distance z, and the asterisk, *, between two functions denotes convolution of the functions. The intensity in the detector plane for the fixed positions x_1 and $x_1 + \Delta x$ of the first and the second optical elements is written as follows,

$$I_{det}(x,y;x_1,\Delta x) = \left|\left(E_{OE1} * P_{R_2}\right)(x,y;x_1)\right|^2 T_2(x - x_1 - \Delta x), \tag{3}$$

where $T_2(x) \equiv |t_2(x)|^2$ is the transmittance function of the second optical element.

We consider the imaging modality in which both optical elements are scanned together (keeping the transverse offset, Δx, constant) along the x-axis while the image is collected. At this stage we should distinguish between two cases: periodic and non-periodic optical elements. If both the optical elements are periodic (e.g. gratings), with period d, then scanning over an integer number of periods is carried out (actually, scanning over one period is sufficient). In the opposite case of non-periodic optical elements (e.g. slits), scanning of the optical elements has to be carried out across the whole horizontal field of view $[-A, A]$. Mathematically, such scanning results in integration of the intensity $I_{det}(x, y; x_1, \Delta x)$ over x_1 in the interval L, equal to $[0, d]$ and $[-A, A]$ in the periodic and non-periodic case, respectively,

$$I_{det}(x,y;\Delta x) \equiv |L|^{-1}\int_L dx_1\, I_{det}(x,y;x_1,\Delta x), \tag{4}$$

where $|L|$ is the length of the interval L. Substituting Eq. (3) into Eq. (4) one obtains,

$$I_{det}(x,y;\Delta x) = \iint dx'dx''\, q_{R_2}(x - x', y)\, q^*_{R_2}(x - x'', y)\, T_x(x', x''; \Delta x), \tag{5}$$

where

$$q_{R_2}(x,y) \equiv \int dy'\, q(x, y - y')\, P_{R_2}(y'), \tag{6}$$

is the result of applying the y-component of the free-space propagator to the object wave and

$$T_x(x', x''; \Delta x) \equiv P_{R_2}(x')\, P^*_{R_2}(x'')\, G(x' - \Delta x, x'' - \Delta x), \tag{7}$$

is a newly introduced propagation function of the imaging system along the x-axis and the function $G(x', x'')$ is defined as

$$G(x', x'') \equiv |L|^{-1}\int_L dX\, t_1(X - x')\, t_1^*(X - x'')\, T_2(X). \tag{8}$$

The Fourier transform of the image intensity distribution over the coordinate x [this is indicated by superscript (1)] is written as follows:

$$\hat{I}^{(1)}_{det}(u,y;\Delta x) = \int du'\, \hat{q}^{(1)}_{R_2}(u + u', y)\, [\hat{q}^{(1)}_{R_2}(u', y)]^*\, \hat{T}_x(u + u', -u'; \Delta x), \tag{9}$$

where the transfer function $\hat{T}_x(u, u'; \Delta x)$ of the imaging system along the x-axis (the Fourier transform of the propagation function of the imaging system) can be presented as

$$\hat{T}_x(u,u';\Delta x) = \iint dw dw'\, \hat{P}_{R_2}(u - w)\, \hat{P}^*_{R_2}(u' - w')\, \hat{G}(w, w') \exp[2\pi i (w + w')\Delta x]. \tag{10}$$

Taking the explicit form of the free-space propagators into account, one obtains an equivalent form for the transfer function,

#92070 - $15.00 USD Received 24 Jan 2008; revised 21 Feb 2008; accepted 21 Feb 2008; published 11 Apr 2008

$$\hat{T}_x(u,u';\Delta x)=\hat{P}_{R_2}(u)\hat{P}^*_{R_2}(u')\iint dwdw'\,\hat{P}_{R_2}(w)\hat{P}^*_{R_2}(w')\hat{G}(w,w') \times\exp\{2\pi i[w(\Delta x+\lambda R_2 u)+w'(\Delta x-\lambda R_2 u')]\}. \tag{11}$$

2.2. Partially coherent incident illumination

Following the same approach that was used in our recent paper [22], we present the cross-spectral density [23] of the incident beam in the following form,

$$\tilde{\Gamma}_{in}(x,y,x',y',\lambda)=W_{in}(x,y,x',y',\lambda)\exp[i\pi(x^2+y^2-x'^2-y'^2)/(\lambda R_1)], \tag{12}$$

where (x, y) and (x', y') are the Cartesian coordinates of two arbitrary points in the object plane and R_1 is the distance from the source to the object. Taking into account transmission through the object and the first grating, propagation from the first to the second grating and transmission through the second grating, the spectral density in the detector plane, located immediately after the second grating, can be expressed as follows,

$$S_{det}(x,y,\lambda;x_1,x_2)=T_2(x-x_2)\iint\iint dXdX'dYdY'W_{in}(X,Y,X',Y',\lambda)(\lambda R_1)^2 P_{R_1}(X,Y)P^*_{R1}(X',Y') \times q(X,Y)q^*(X',Y')t_1(X-x_1)t_1^*(X'-x_1)P_{R_2}(x-X,y-Y)P^*_{R_2}(x-X',y-Y'), \tag{13}$$

where $x_{1,2}$ are the positions along the x-axis of the first and second gratings respectively. Equation (13) can be straightforwardly transformed to the equivalent form,

$$M^2S_{det}(Mx,My,\lambda;x_1,x_2)=T_2(Mx-x_2)\iint\iint dXdX'dYdY'W_{in}(X,Y,X',Y',\lambda)q(X,Y)q^*(X',Y') \times t_1(X-x_1)t_1^*(X'-x_1)P_{R'}(x-X,y-Y)P^*_{R'}(x-X',y-Y'), \tag{14}$$

where $M\equiv(R_1+R_2)/R_1$ is the geometrical magnification of the imaging system and $R'\equiv R_1R_2/(R_1+R_2)$ is the effective object-to-detector distance.

Following reference [22] we consider a model for partially coherent incident illumination which represents a generalization of the Schell model (for which the spatial coherence properties in the plane of incidence depend only on the distance between the points in this plane). According to this model the function W_{in} in the incident cross-spectral density has the following form,

$$W_{in}(x,y,x',y',\lambda)=S^{1/2}_{in}(x,y,\lambda)S^{1/2}_{in}(x',y',\lambda)g_{in}(x-x',y-y',\lambda) \times\exp\{i[\varphi_{in}(x,y,\lambda)-\varphi_{in}(x',y',\lambda)]\}, \tag{15}$$

where S_{in} is the spectral density of the incident wave and we allowed for an additional phase term φ_{in} in the incident wave (apart from the explicit parabolic term in Eq. (12)). Substituting Eq. (15) into Eq. (14), one obtains

$$M^2S_{det}(Mx,My,\lambda;x_1,x_2)=T_2(Mx-x_2)\iint\iint dXdX'dYdY'\,g_{in}(X'-X,Y'-Y,\lambda)Q(x-X,y-Y) \times Q^*(x-X',y-Y')t_1(x-X-x_1)t_1^*(x-X'-x_1)P_{R'}(X,Y)P^*_{R'}(X',Y'), \tag{16}$$

where we have introduced a modified transmission function $Q\equiv S^{1/2}_{in}\exp(i\varphi_{in})q$. Assuming that $x_2 = Mx_1 + M\,\Delta x$ and integrating Eq. (16) over x_1 (therefore the second optical element is shifted M times faster than the first one), one obtains the following expression for the spectral density in the detector plane,

$$M^2S_{det}(Mx,My,\lambda;\Delta x)=\iint\iint dXdX'dYdY'T_{sys}(X,Y,X',Y';\lambda,\Delta x)Q(x-X,y-Y) \times Q^*(x-X',y-Y'), \tag{17}$$

where the propagation function of the system has been introduced,

#92070 - $15.00 USD Received 24 Jan 2008; revised 21 Feb 2008; accepted 21 Feb 2008; published 11 Apr 2008

$$T_{sys}(x,y,x',y';\lambda,\Delta x) \equiv g_{in}(x'-x,y'-y,\lambda)P_{R'}(x,y)P_{R'}^{*}(x',y')G(x-\Delta x,x'-\Delta x), \quad (18)$$

and by analogy with the case of an incident plane wave, the function $G(x,x')$ is defined as

$$G(x,x') \equiv |L|^{-1}\int_{L} dX\, t_1(X-x)t_1^{*}(X-x')T_2(MX), \quad (19)$$

where the integration interval L was defined in section 2.1. Fourier transforming to Eq. (17), one easily obtains the following general expression,

$$\hat{S}_{det}(u/M,v/M,\lambda;\Delta x) = \iint dUdV\,\hat{T}_{sys}(u+U,v+V,-U,-V;\lambda,\Delta x)\hat{Q}(u+U,v+V)\hat{Q}^{*}(U,V). \quad (20)$$

The transfer function of the imaging system, $\hat{T}_{sys}(u,v,u',v';\lambda,\Delta x)$, corresponds to partially coherent incident illumination characterized by the spectral degree of coherence $g_{in}(x'-x,y'-y,\lambda)$ that, according to the generalized Schell model used in this paper, depends only on the distance between two arbitrary points (x,y) and (x',y') in the plane of incidence. This "partially coherent" transfer function can be expressed in terms of the "ideal" transfer function, $\hat{T}_{id}(u,v,u',v';\lambda,\Delta x)$, that corresponds to coherent incident illumination with $g_{in} \equiv 1$, as

$$\hat{T}_{sys}(u,v,u',v';\lambda,\Delta x) = \iint dUdV\ \hat{g}_{in}(U,V,\lambda)\hat{T}_{id}(u+U,v+V,u'-U,v'-V;\lambda,\Delta x). \quad (21)$$

One practically important case is that of an extended spatially incoherent source [23], characterized by a normalized spectral density distribution in the source plane, $S_{src}(x,y,\lambda)$. It results in Schell-type incident illumination characterized by a uniform spectral density function, $S_{in} = S_{in}(\lambda)$, and by a spectral degree of coherence related to the spectral density distribution in the source plane via a rescaled Fourier transform,

$$g_{in}(\Delta x,\Delta y,\lambda) = \hat{S}_{src}[-\Delta x/(\lambda R_1),-\Delta y/(\lambda R_1),\lambda]. \quad (22)$$

Given the spectral density distribution in the detector plane, $S_{det}(x,y,\lambda;\Delta x)$, the corresponding intensity distribution $I_{det}(x,y;\Delta x)$ in the detector plane is calculated as follows,

$$I_{det}(x,y;\Delta x) = \int d\lambda\, S_{det}(x,y,\lambda;\Delta x). \quad (23)$$

Formation of a quasi-monochromatic image in the proposed scanning double-grating imaging method is described by Eq. (17), which is mathematically identical to that obtained in the case of a polychromatic analyser-based imaging [24]. *Therefore the object wave phase/amplitude reconstruction algorithms* [24] *developed for analyser-based imaging (using either the weak-object approximation or the geometrical-optics approximation) can be successfully applied to the scanning double-grating imaging, though with a different definition for the transfer function of the imaging system.*

2.3. Geometrical optics approximation

Equation (17) can be equivalently presented as follows,

$$\begin{aligned} M^2 S_{det}(Mx,My,\lambda;\Delta x) = {} & \iint dXdX' \iint dYdY' Q(X,Y)Q^{*}(X',Y') \\ & \times \iint dUdU' \exp\{-2\pi i[U(x-X)+U'(x-X')]\} \\ & \times \iint dVdV' \exp\{-2\pi i[V(y-Y)+V'(y-Y')]\} \\ & \times \hat{T}_{sys}(U,V,U',V';\lambda,\Delta x). \end{aligned} \quad (24)$$

#92070 - $15.00 USD Received 24 Jan 2008; revised 21 Feb 2008; accepted 21 Feb 2008; published 11 Apr 2008

Assume that the object transmission function Q is slowly varying compared to the system transmission function T_{sys}. Then applying the stationary-phase method [25] to the eight-fold integral in Eq. (24) and preserving only the first term in the corresponding decomposition formula (thus neglecting the in-line contrast and the diffraction effects due to the intensity variations in the object wave), one obtains the geometrical-optics approximation for the spectral density in the detector plane,

$$M^2 S_{det}(Mx, My, \lambda; \Delta x) \cong S_0(x, y, \lambda)\, \hat{T}_{sys}(u_0, u_0, -u_0, -u_0; \lambda, \Delta x), \tag{25}$$

where $S_0 \equiv |Q|^2 = S_{in}\,|q|^2$, $\varphi \equiv \arg(Q)$ and $u_0 \equiv -(2\pi)^{-1}\partial_x \varphi(x, y)$. Note that a similar result has been obtained for the analyzer-based imaging system [24].

According to Eq. (11) and Eq. (21), the system transfer function in Eq. (25) can be presented alternatively in the following simple form

$$\hat{T}_{sys}(u_0, u_0, -u_0, -u_0; \lambda, \Delta x) \equiv r_{sys}[(\Delta x / R') + \lambda u_0], \tag{26}$$

where $r_{sys}(\theta) \equiv \iint dU dV\ \hat{g}_{in}(U, V, \lambda)\, r_{id}(\theta + \lambda U)$ and $r_{id}(\theta) \equiv \hat{T}_{id}(0,0,0,0; \lambda, R'\theta)$. The newly introduced functions $r_{sys}(\theta)$ and $r_{id}(\theta)$ are analogous to the rocking curve and the intrinsic reflectivity curve of the analyzer crystal in analyzer-based imaging, respectively [24].

In order to calculate the intensity distribution in the detector plane, one needs to integrate the spectral density distribution over the wavelength, Eq. (23). We should emphasize that all distributions in Eq. (25), including u_0, depend on the wavelength. In order to obtain a formula for the intensity distribution in the detector plane that could be used for the phase/amplitude reconstruction of the object wave, we introduce the following assumptions. We assume that the spectrum of the incident beam is narrow, so that $\Delta\lambda/\lambda < 0.1$, and is far from the absorption edges of the materials constituting the object and the gratings. Then introducing the refraction angle, $\alpha(x,y;\lambda) \equiv \lambda u_0(x,y;\lambda)$, and the absorption function of the object, $b(x,y;\lambda) \equiv -(1/2)\ln(|q(x,y;\lambda)|^2)$, both the refraction angle and the absorption function can be well approximated using the following linear decompositions,

$$\alpha_x(x, y; \lambda) \cong \alpha_x(x, y; \lambda_0)(1 + 2\varepsilon), \quad b(x, y; \lambda) \cong b(x, y; \lambda_0)[1 + k(x, y)\,\varepsilon], \tag{27}$$

where $\varepsilon \equiv \lambda / \lambda_0 - 1 < 0.1$, λ_0 is some 'central' value of the wavelength (an exact definition for the λ_0 is derived below), and $k(x,y)$ is the slope coefficient of the absorption function for a point (x,y) in the object plane (its value depends on the chemical composition of the object's voxels contributing to the absorption at this point of the object plane).

Assuming further that the refraction angles do not exceed a period of the rocking curve $r_{sys}(\theta)$ of the imaging system and that the absorption function of the object does not exceed one, the product $2\varepsilon\,\alpha(x,y;\lambda_0)$ is small compared to the period of the rocking curve and the product $2\varepsilon\, b(x,y;\lambda_0)\, k(x,y)$ is small compared to one. This allows us to present the right-hand-side of Eq. (26) and the transmission function of the object, $\exp[-2b(x,y;\lambda)]$, as follows ($\theta_0 \equiv \Delta x/R'$),

$$\begin{aligned} r_{sys}[\theta_0 + \alpha(x, y; \lambda); \lambda] \cong\ & r_{sys}[\theta_0 + \alpha(x, y; \lambda_0); \lambda] \\ & + 2\varepsilon\,\alpha(x, y; \lambda_0)\, r'_{sys}[\theta_0 + \alpha(x, y; \lambda_0); \lambda], \end{aligned} \tag{28}$$

$$\exp[-2b(x, y; \lambda)] \cong \exp[-2b(x, y; \lambda_0)][1 - 2b(x, y; \lambda_0)\, k(x, y)\, \varepsilon]. \tag{29}$$

Substituting Eq. (28) and Eq. (29) into Eq. (25) and integrating over the wavelength, one obtains the following approximate expression for the intensity distribution in the detector plane (we assume, for simplicity, that the incident spectral density can be factorised into spatial and spectral terms, viz $S_{in}(x, y;\lambda) = S_{in,spat}(x, y)\, S_{in,spec}(\lambda)$),

#92070 - $15.00 USD Received 24 Jan 2008; revised 21 Feb 2008; accepted 21 Feb 2008; published 11 Apr 2008

$$M^2 I_{det}(Mx, My; \Delta x) \cong S_{in,spat}(x, y) \exp[-2b(x, y; \lambda_0)] \Big(r_{sys,poly}[\theta(x, y; \lambda_0)] + 2 \int d\lambda \, S_{in,spec}(\lambda) \varepsilon \{ \alpha(x, y; \lambda_0) \, r'_{sys}[\theta(x, y; \lambda_0); \lambda] - b(x, y; \lambda_0) \, k(x, y) \, r_{sys}[\theta(x, y; \lambda_0); \lambda] \} \Big) \tag{30}$$

where $\theta(x, y; \lambda_0) \equiv \theta_0 + \alpha(x, y; \lambda_0)$. It is convenient to choose the 'central' wavelength $\lambda_0 = \lambda_0(x,y)$ such that the integral over λ in Eq. (30) is zero. Then the image formation in the polychromatic geometrical-optics approximation is described by the following simple formula,

$$M^2 I_{det}(Mx, My; \Delta x) \cong S_{in,spat}(x, y) \exp[-2b(x, y; \lambda_0)] \, r_{sys,poly}[\theta_0 + \alpha(x, y; \lambda_0)], \tag{31}$$

where the polychromatic rocking curve is defined as follows,

$$r_{sys,poly}(\theta) \equiv \int d\lambda \, r_{sys}(\theta; \lambda) \, S_{in,spec}(\lambda) \, . \tag{32}$$

We should note one practically important case a narrow spectrum of the incident beam (in accordance with our assumption above). In this case, the rocking curve and its derivative are even functions of a small wavelength shift $\Delta\lambda$ with respect to the wavelength λ_T for which the Talbot self-imaging condition is satisfied (see Eq. (45) below). If the spectrum distribution $S_{in,spec}(\lambda)$ is an even function with respect to some wavelength λ_c (this is the mean wavelength in the spectrum) then by choosing $\lambda_T = \lambda_c$, the integral in Eq. (30) is equal to zero for all refraction angles α if the wavelength λ_0 is chosen to be equal to λ_c. Then applying Eq. (31) to the reconstruction of the refraction angle distribution $\alpha(x,y)$ and the absorption function $b(x,y)$, both these reconstructed distributions correspond to the wavelength λ_c. Equation (31) closely resembles the geometrical-optics approximation in analyzer-based imaging [24].

3. Scanning double-grating imaging using partially coherent incident illumination

In this section we apply our general results, Eqs. (17)-(21), to the scanning-based imaging system consisting of two gratings. Let d be the period of the first grating and let Md be the corresponding period of the second grating. It is convenient to present both the transmission function $t_1(x)$ of the first grating and the transmittance function $T_2(x)$ of the second grating in the form of Fourier series,

$$t_1(x) = \sum_n a_n \exp(-2\pi i nx / d), \qquad T_2(x) = \sum_n b_n \exp[-2\pi i nx / (Md)], \tag{33}$$

where the Fourier coefficients are defined in general as follows,

$$a_n = d^{-1} \int_0^d dx \exp(2\pi i nx / d) t_1(x),$$

$$b_n = (Md)^{-1} \int_0^{Md} dx \exp[2\pi i nx / (Md)] T_2(x) = d^{-1} \int_0^d dx \exp(2\pi i nx / d) T_2(Mx). \tag{34}$$

Substituting Eq. (33) into Eq. (19) with $L = [0, d]$, one obtains,

$$G(x, x') = \sum_n \sum_m a_n a_m^* b_{m-n} \exp[2\pi i (nx - mx') / d]. \tag{35}$$

The "ideal" transfer function of the double-grating imaging system (corresponding to coherent incident illumination) is then obtained by taking the Fourier transform of Eq. (18) with $g_{in} = 1$, giving

#92070 - $15.00 USD Received 24 Jan 2008; revised 21 Feb 2008; accepted 21 Feb 2008; published 11 Apr 2008

$$\hat{T}_{id}(u,v,u',v';\lambda,\Delta x)=\sum_n\sum_m a_n a_m^* b_{m-n}\exp[2\pi i(m-n)\Delta x/d]\hat{P}_{R'}(u+n/d,v)\times\hat{P}_{R'}^*(u'-m/d,v'). \tag{36}$$

Substituting Eq. (36) into Eq. (21), one obtains

$$\hat{T}_{sys}(u,v,u',v';\lambda,\Delta x)=\sum_n\sum_m a_n a_m^* b_{m-n}\exp[2\pi i(m-n)\Delta x/d]\hat{P}_{R'}(u+n/d,v)\times\hat{P}_{R'}^*(u'-m/d,v')g_{in}[\lambda R'(u+n/d+u'-m/d),\lambda R'(v+v'),\lambda]. \tag{37}$$

Comparison of Eq. (36) and Eq. (37) shows that effect of partial coherence for the generalized Schell-model incident illumination results in the appearance of the damping factor in Eq. (37) which is merely a rescaled spectral degree of coherence.

Calculation of the grating-based images simplifies significantly if the spectral degree of coherence allows factorization with respect to Δx and Δy, i.e.

$$g_{in}(\Delta x,\Delta y,\lambda)=g_{in,x}(\Delta x,\lambda)g_{in,y}(\Delta y,\lambda).$$

Then Eq. (20) can be simplified to what follows, namely

$$\hat{S}_{det}(u/M,v/M,\lambda;\Delta x)=g_{in,y}(\lambda R'v,\lambda)\hat{S}_{\perp}(u,v,\lambda;\Delta x), \tag{38}$$

where $\hat{S}_{\perp}(u,v,\lambda;\Delta x)$ and $\hat{T}_x(u,u';\lambda,\Delta x)$ are defined below,

$$\hat{S}_{\perp}^{(1)}(u,y,\lambda;\Delta x)\equiv\int dU\,\hat{Q}_{R'}^{(1)}(u+U,y)\left[\hat{Q}_{R'}^{(1)}(U,y)\right]^*\hat{T}_x(u+U,-U;\lambda,\Delta x), \tag{39}$$

$$\hat{T}_x(u,u';\lambda,\Delta x)=\sum_n\sum_m a_n a_m^* b_{m-n}\exp[2\pi i(m-n)\Delta x/d]\hat{P}_{R'}(u+n/d)\times\hat{P}_{R'}^*(u'-m/d)g_{in,x}[\lambda R'(u+n/d+u'-m/d),\lambda]. \tag{40}$$

In Eq. (39) $Q_{R'}$ designates a result of applying only the y-component of the free-space propagator to the object transmission function (y-axis is parallel to the grating lines),

$$Q_{R'}(x,y)\equiv\int dY\,Q(x,y-Y)P_{R'}(Y), \tag{41}$$

and the superscript (1) denotes that the corresponding Fourier transform is taken over the first spatial variable.

4. Numerical results and discussion

In the point-projection geometry with magnification M, the effective source size in the object plane is expressed via the source size, w_S (FWHM), as follows

$$w_{S,\mathrm{eff}}=w_S(1-M^{-1}). \tag{42}$$

We should emphasize that the effective source size does not exceed the actual source size at any magnification $M\geq 1$.

Visibility of a self-image formed by the first grating remains good if the effective source size is much smaller than the period d of the self-image (referred hereafter to the object plane), i.e.

$$w_{S,\mathrm{eff}}\leq nd, \tag{43}$$

where n should be sufficiently smaller than one (n = 1/8 found to be sufficient).

Depending on the X-ray source size, two practically important cases can be distinguished:

#92070 - $15.00 USD Received 24 Jan 2008; revised 21 Feb 2008; accepted 21 Feb 2008; published 11 Apr 2008

1. source size does not exceed the critical value, $w_S \le nd$;
2. source size is larger than the critical value, $w_S > nd$.

Below we consider separately these two cases. In our numerical results presented in this section we assume a rectangular profile for both gratings with assumed line-to-space ratio 1:1.

4.1. Small X-ray source

We assume that the source size does not exceed the critical value,

$$w_S \le nd. \tag{44}$$

Then there is no limit on the magnification of the system. The imaging system configuration is built based on the following considerations. The Talbot distances, i.e. the distances downstream from the first grating at which the grating produces so-called fractional Talbot self-images, are given as follows [16]

$$z_m = md_1^2 /(2\eta^2 \lambda) , \tag{45}$$

where d_1 is a period of the first grating, the integer number m is the Talbot order which should be odd for a phase grating and even for an amplitude grating. The factor η depends on the choice of the first grating. In the case of either a phase grating with the phase modulation $\varphi_0 = \pi/2$ or an amplitude grating the corresponding value is $\eta = 1$. In this case the period of the self-image is equal to the period of the first grating, $d = d_1$. Another widely used configuration corresponds to the first phase grating having phase modulation $\varphi_0 = \pi$. In this case the corresponding value of the factor is $\eta = 2$ and the period of the self-image is half of the first grating period, i.e. $d = d_1/2$. In both cases, $d = d_1/\eta$ and the period of the second (amplitude) grating is chosen to be equal to the period of the corresponding self-image multiplied by the magnification, i.e. $d_2 = M\, d_1/\eta$.

On the other hand, the effective object-to-detector propagation distance, R', is expressed via the magnification, M, and the source-to-detector distance, R, as follows,

$$R' = M^{-2}(M-1)R . \tag{46}$$

It is assumed that period d_2 of the amplitude grating is an independent parameter. Then the period of the phase grating is defined as follows, $d_1 = \eta\, d_2 / M$. Equating R', given by Eq. (46), to the Talbot distance z_m, Eq. (45), one can easily obtain the following equation for the appropriate magnification as a function of d_2, λ and R,

$$M = 1 + md_2^2 /(2\lambda R) . \tag{47}$$

The ability of the grating-based imaging system to detect small deflections of the wave propagated through the object depends on the angular acceptance of the period of the self-image as seen from the object, i.e. d/R'. The smaller this ratio the more the GBI system is sensitive to small deflection angles. This angular acceptance can be presented in terms of d_2, λ and R as follows,

$$d / R' = d_2 / R + 2\lambda /(md_2) . \tag{48}$$

Analysis of Eq. (48) shows that for fixed R and λ, the ratio d/R' has large values for both small and large values of d_2 and has a minimum at the optimum value of d_2,

$$(d_2)_{opt} = (2\lambda R / m)^{1/2} , \quad (d / R')_{\min} = 2[2\lambda /(mR)]^{1/2} . \tag{49}$$

Equation (49) indicates that the angular acceptance of the self-image period can be improved (decreased) by either decrease of the x-ray wavelength λ or by increase of the total distance R. Note, however, that the deflection angles due to the object are inversely

#92070 - $15.00 USD Received 24 Jan 2008; revised 21 Feb 2008; accepted 21 Feb 2008; published 11 Apr 2008

proportional to the second power of λ which results in decrease in the image contrast for smaller wavelengths, as $\lambda^{3/2}$. On the other hand, only a large increase in the total distance can result in significant improvement of the contrast (for example, in order to double the differential contrast, R should be increased four times). It should be mentioned that according to Eq. (47), the optimum period of the second grating $(d_2)_{opt}$ corresponds to magnification $M = 2$ independently of the x-ray energy and total distance. According to Eq. (44), the maximum allowable source size corresponding to the optimum period $(d_2)_{opt}$ is $w_{S,\max} = (n/2)(2\lambda R/m)^{1/2}$. Remarkably, the optimum period $(d_2)_{opt}$ not only minimises the ratio d/R' but also maximises the period of the self image d, namely

$$d_{\max} = (d_2)_{opt}/2 . \tag{50}$$

As an example we consider the case where $R = 250$mm, $d_2 = 24$ m, $\lambda = 3$Å and $m = 1$. Then according to Eq. (47) the corresponding magnification is $M = 4.84$. At the same time the source size should satisfy Eq. (44); assuming $n = 1/8$ this gives $w_S \le 0.62$ m. These and other important geometrical parameters are summarized in Table 2 below. Some simulated images of a spherical pure phase object of diameter 0.5mm (maximum phase shift is 12 radians at the wavelength $\lambda = 3$Å) which was radially smeared using a Gaussian function with 100 m FWHM are shown in Fig. 2. The contrast in the images was calculated using the following formula, $C' \equiv (I_{\max} - I_{\min})/2$, where $I_{\max}$ and $I_{\min}$ are correspondingly the maximum and minimum intensity values in the images of the object (hereafter a unit intensity of the incident wave is assumed).

Table 2. Geometrical parameters of the double-grating imaging system with $R = 250$mm and satisfying the fractional Talbot condition, eq.(45), with $m = 1$, for different values of d_2 and λ.

d_2, m	λ, Å	M	d, m	w_S, m	R', mm	R_1, mm	R_2, mm	d/R', ″	C', %
6	3	1.24	4.84	0.605	39.02	201.6	48.4	25.6	5.91
12	3	1.96	6.12	0.765	62.47	127.6	122.4	20.2	7.47
24	3	4.84	4.96	0.62	40.98	51.7	198.3	25	6.05
48	3	16.36	2.93	0.37	14.35	15.3	234.7	42.1	3.59
9	1.5	2.08	4.327	0.541	62.41	120.2	129.8	14.3	2.65
12	1.5	2.92	4.11	0.51	56.30	85.6	164.4	15.1	2.51

Analysis of Eqs. (47)-(50) and of the data in Table 2 and Fig. 2 allowed us to reveal the following trends in SDG imaging using an ultra small X-ray source and a fixed source-to-detector distance. First, given the X-ray energy fixed (e.g. $\lambda = 3$Å), the magnification M changes almost as the second power of the period d_2 of the second (amplitude) grating: $M = 1.96$ in the case of $d_2 = 12$ m, $M = 4.84$ in the case of $d_2 = 24$ m and $M = 16.36$ in the case of $d_2 = 48$ m. The first of the above three values of d_2, namely $d_2 = 12$ m is close to the optimum value, Eq. (49), $(d_2)_{opt} = 12.25$ m for the chosen $R = 250$mm and $\lambda = 3$Å. The maximum source size and contrast decrease when d_2 deviates from $(d_2)_{opt}$.

Second, the above two schemes, corresponding to the two values of the phase modulation of the phase grating, $\pi/2$ and π, are virtually identical. The only difference is in the period of the phase grating. It is twice larger in the scheme with phase modulation equal to π. Note, however, that the aspect ratio in the height profile of the phase grating is the same for both cases as the twice larger phase modulation is achieved by two times higher thickness profile in the phase grating.

Third, increase of X-ray energy (given the amplitude grating period fixed) results in decrease of the period of the self-image, decrease of the maximum allowable source size and significant decrease of the contrast in the images (compare Fig. 2(c) and Fig. 2(d)). The latter

#92070 - $15.00 USD Received 24 Jan 2008; revised 21 Feb 2008; accepted 21 Feb 2008; published 11 Apr 2008

means that there is a trade-off between radiation dose absorbed by an object and the effectiveness of the SDG imaging.

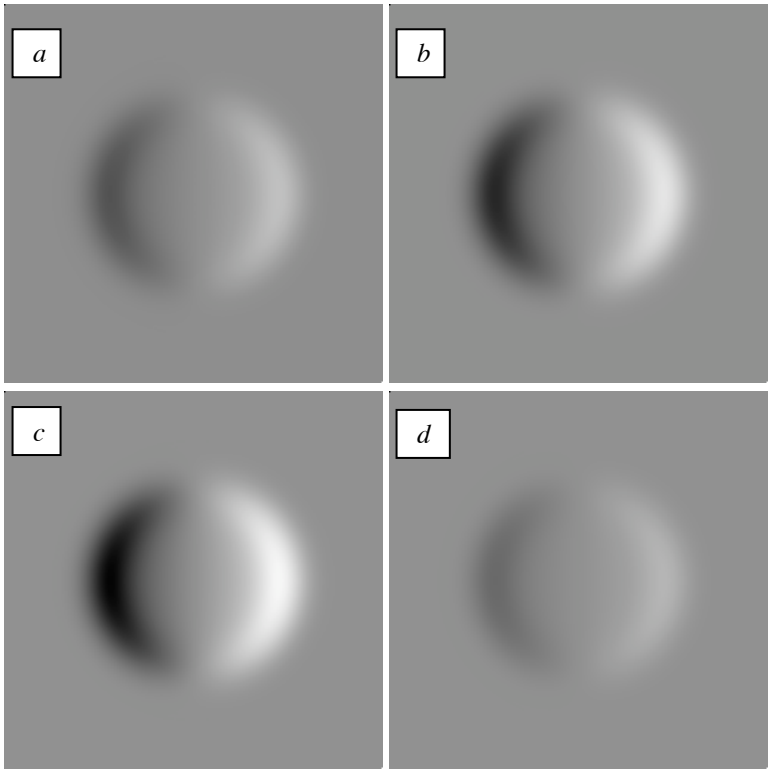

Fig. 2. Simulated SDG images with $\Delta x = d/4$ of a model object described in the text using geometrical parameters from Table 2: $\lambda = 3$Å and $d_2 = 48$ m (a), 24 m (b) and 12 m (c); $\lambda = 1.5$Å and $d_2 = 12$ m (d). A finite source, $w_S = d/8$, and an ideal detector have been used in our calculations. White (black) corresponds to the maximum (minimum) displayed intensity; the difference between the maximum and minimum displayed intensity is 0.16 in all images.

4.2. Large X-ray source

Now consider a case where the source size is larger than the critical value,

$$w_S > nd. \tag{51}$$

In this case demagnification of the source is needed, and the effective source size in the object plane is given by Eq. (42). It follows immediately from Eq. (42) and Eq. (43) that the maximum magnification which satisfies the condition that the effective source size does not exceed the critical size nd is written as follows,

$$M_{\max} = (1 - nd / w_S)^{-1}. \tag{52}$$

According to Eq. (52), at a given self-image period, the larger the source size the closer to one the magnification should be. Considering the period $d_2 = Md$ of the second (amplitude) grating as an independent variable, the maximum magnification that still satisfies Eq. (43) is written as follows,

$$M_{\max} = 1 + nd_2 / w_S . \tag{53}$$

The general expressions for the total distance, R, and the angular acceptance of the period of the self-image, d/R', are written in terms of d_2, λ and M as follows,

#92070 - $15.00 USD Received 24 Jan 2008; revised 21 Feb 2008; accepted 21 Feb 2008; published 11 Apr 2008

$$R = md_2^2 / \left[2\lambda(M-1)\right], \quad d / R' = 2\lambda M / (md_2). \tag{54}$$

Equation (54) indicates opposite dependencies of the total distance and angular acceptance on each of the three parameters, d_2, λ and M. For example, in terms of magnification, the maximum allowable magnification, Eq. (53), minimizes the total distance and if one assumes that the $M_{\max}$ does not exceed 2, then the maximum increase of the ratio d/R' due to the magnification is 2 (note that the optimum magnification minimizing this ratio is 1). In the following we shall assume that $M = M_{\max}$ which results in the transformation of Eq. (54) to

$$R = md_2 w_S / (2n\lambda), \quad d / R' = (2\lambda / m)[(1/d_2) + (n / w_S)]. \tag{55}$$

Equation (55) shows that the total distance can only be decreased by decreasing the source size, w_S, decreasing the second grating period, d_2, or increasing the x-ray wavelength λ. However, decrease of both w_S and d_2 results in increase of the ratio d/R' and, as a result, in decrease of the contrast. Notwithstanding the increase of the ratio d/R' with the x-ray wavelength, the overall effect of the wavelength is positive for the contrast (differential contrast is proportional to λ). Note, however, that the total absorbed dose increases significantly with increase of λ (the linear absorption coefficient is approximately proportional to λ^3). Thus there are two definite tradeoffs, the first one is between the contrast and the total distance, and the second one is between the contrast and the absorbed dose.

Some example calculations of the geometrical parameters based on Eqs. (52)-(55) are given in Table 3 below.

Table 3. Geometrical parameters of the double-grating imaging system with $m = 1$.

w_S, m	d_2, m	λ, Å	$M_{\max}$	d, m	R', mm	d/R',″	R, mm	R_2, mm[a]
100	16	1	1.02	15.69	1230.3	2.63	64,000	1254.9
100	8	1	1.01	7.92	313.69	5.21	32,000	316.8
100	4	1	1.005	3.98	79.21	10.36	16,000	79.6
10	8	1	1.1	7.27	264.46	5.67	3,200	290.9
5	16	1	1.4	11.43	653	3.61	3,200	914.3
5	8	0.5	1.2	6.67	444	3.10	3,200	532.8
5	8	1	1.2	6.67	222	6.19	1,600	266.4
5	4	1	1.1	3.64	66.1	11.36	800	72.7

[a] $R_2 = m\, d_2^2 / (2\lambda)\, [1 + nd_2 / w_S]^{-1}$

The following three practically important trends can be established by analysis of Eqs. (53)-(55) and data in Table 3. First, if the period of the second grating and the X-ray wavelength are fixed and the source size is increased, the self-image period d and the distance R_2 between the gratings increase only slightly. Also, according to Eq. (55), the total source-to-detector distance, R, is proportional to the source size. At the same time, the angular acceptance, d/R', slightly decreases with increasing source size; this results only in slight improvement of the contrast in the SDG images. Thus, in order to use grating-based imaging in laboratory conditions (with the total source-to-detector distance limited to several meters) the source size should not exceed ~10 m. If the total source-to-detector distance can be made significantly larger, of the order of 20-100m (as at synchrotrons) then the source size can be of the order of 100 m which is typical for most modern synchrotrons. Note however that the potential improvement in the contrast achievable by going to large distances and large sizes of the source is quite moderate. The greatest advantage of using synchrotron sources is the many orders of magnitude higher intensity in the incident beam. In order to be able to use standard (laboratory) X-ray sources (with the focus size of the order of several hundred microns), an

#92070 - $15.00 USD Received 24 Jan 2008; revised 21 Feb 2008; accepted 21 Feb 2008; published 11 Apr 2008

additional amplitude grating $G0$ should be mounted in front of the source [8,14]. The period of this grating is calculated according to the following formula, $d_0 = (R_1 / R_2)\, d_2$. Such a grating produces an array of line sourcelets whose width (the width of a transparent part of the grating period) should be chosen appropriately, according to our considerations above. This would guarantee high performance of the gratings (visibility of fringes in the self-image and contrast in the image of the object formed by each individual sourcelet). Note, however, that the total spatial resolution of the system in this case is limited by the total source size, not the size of an individual sourcelet.

Second, given fixed source size and the X-ray wavelength, decreasing the amplitude grating period d_2 results in the period of the self-image decreasing almost linearly with d_2. Also, and more importantly, the distance R_2 between the gratings decreases almost as the second power of d_2. This reduction in the distance between the gratings is, however, accompanied by linear increase of the ratio d/R' and results in linear decrease of the contrast in the images. The source-to-detector distance R also decreases linearly with decrease of d_2. Thus, the amplitude and phase grating with small period are preferable if one needs to minimize the overall size of the SDG imaging system. Note however that this compactness is achieved at the expense of the system effectiveness (contrast in the images).

Third, decrease of X-ray wavelength (by using more energetic X-rays) does not affect the self-image period but results in inversely proportional increase of both the R and R_2. Notwithstanding that the ratio d/R' decreases two times given the two times decrease of the wavelength, the contrast in the SDG images decreases two times. This effect is shown in Fig. 3 where the simulated images of a spherical object of diameter 0.5mm, radially smeared using a Gaussian function with 100 m FWHM, are shown. The observed reduction of contrast in the image calculated using 0.5Å wavelength as compared to the image calculated using 1Å wavelength is due to the fact that the deflection angles induced by the object decrease four times. This is because the deflection angle is proportional to the second power of the wavelength. Thus, by increasing X-ray energy, on the one hand, one can deliver significantly smaller radiation dose to the sample (the linear absorption coefficient is inversely proportional to the third power of the X-ray energy); on the other hand, performance of the imaging system (contrast in the images) decreases linearly with increasing X-ray energy.

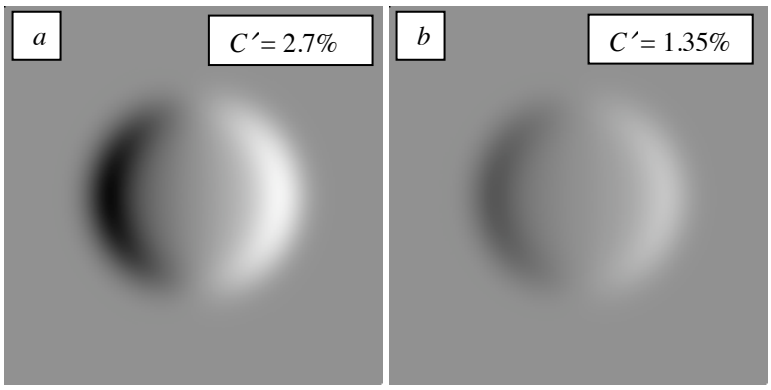

Fig. 3. Simulated SDG images with $\Delta x = d/4$ of a model object described in the text using geometrical parameters corresponding to $w_S = 5$ m, $d_2 = 8$ m and two values of λ: 1Å (a) and 0.5Å (b). The difference between the minimum and maximum displayed intensity is 0.06 for both the images (unit intensity of the incident wave is assumed).

4.3. Effect of polychromaticity on the SDG image formation

The effect of polychromaticity of X-ray radiation incident on the object is investigated in terms of its influence on scanning double-grating imaging. The following three issues have to be taken into account when dealing with polychromatic incident radiation [13,17]:

#92070 - $15.00 USD Received 24 Jan 2008; revised 21 Feb 2008; accepted 21 Feb 2008; published 11 Apr 2008

1. The complex transmission function of an object is wavelength dependent. In the simplest case of the whole spectrum of the source being far from the absorption edges of the materials constituting the object, a phase induced by the object varies linearly with the wavelength and an absorption coefficient varies as the third power of the wavelength.
2. The phase induced by the first (phase) grating varies linearly with the X-ray wavelength (assuming that the whole spectrum of the source is far from the absorption edges of the material of the phase grating). Thickness of the lines in the second (amplitude) grating is assumed to be sufficiently large so that the transmittance of the lines in the grating is zero for all the energies in the spectrum of the source.
3. The Talbot distances are inversely proportional to the X-ray wavelength. Therefore, if the distance between the gratings is equal to one of the Talbot distances for a particular wavelength and a self-image is observed for that wavelength, the chosen (fixed) distance does not coincide with Talbot distances for other wavelengths.

The first and the third issues have been addressed by Momose et al. **[17]**. Based on simple considerations, they have formulated the following condition for the maximum allowable polychromaticity in the standard (non-scanning) grating-based imaging approach with $\varphi_0 = \pi/2$,

$$\Delta\lambda/\lambda < 1/8. \tag{56}$$

Weitkamp et al. [13] have shown that in the double-grating scheme with the phase shift modulation $\varphi_0 = \pi$ the maximum allowable polychromaticity, that preserves efficiency of the interferometer, is defined as follows,

$$\Delta\lambda/\lambda < 1 / (2m - 1), \tag{57}$$

where $m = 1, 3, 5, \ldots$ is the order of the Talbot distance used. We should note however that dispersion in the object (sample) and in the gratings was ignored in this estimation (the dispersion effects in the gratings were assessed in [13] using numerical simulations).

In order to provide some quantitative insight into the problem of the effect of polychromaticity on SDG image formation, the following numerical simulations have been carried out. Images of a simple pure phase spherical object with the diameter 0.5mm smeared with a 100 m (FWHM) Gaussian function have been calculated using rigorous wave-optical formalism. The maximum phase shift due to the object at the wavelength $\lambda = 3$Å was 12 radians. The phase modulation in the first (phase) grating was $\pi/2$ at the wavelength 3Å. The period d of the gratings was 8 m. The corresponding Talbot distance was calculated using Eq. (45) with $m = 1$ and $\eta = 1$, $z_1 = d^2/(2\lambda) = 0.107$m.

Several spectral density distributions in energy (Gaussian distributions for the wavelength with the mean value 3Å and different FWHM, $\Delta\lambda$) have been generated (see Fig. 4(a)). The differential ($\Delta x = d/4$) and dark-field ($\Delta x = d/2$) images of the model object have been calculated assuming monochromatic incident radiation as well as using the generated spectra. Some characteristics of the images (including minimum and maximum intensities and the contrast) are summarized in Table 4. The dark-field images are shown in Fig. 5.

Table 4. Some characteristics of the images of the model object described in the text.

	Differential contrast				Dark-field contrast			
$\Delta\lambda/\lambda$	$I_{\min}$	$I_{\max}$	I_{BG}	C', (%)	$I_{\min}$	$I_{\max}$	I_{BG}	C', (%)
0	0.3944	0.5898	0.4929	9.77	0.007108	0.09192	0.007112	4.24
0.1	0.3962	0.588		9.59	0.04771	0.08554	0.04804	1.89
0.2	0.3892	0.595		10.29	0.07103	0.09974	0.07156	1.44
0.4	0.3776	0.6066		11.45	0.1091	0.1301	0.1099	1.05
0.8	0.39	0.594		10.2	0.1695	0.1913	0.1708	1.09

#92070 - $15.00 USD Received 24 Jan 2008; revised 21 Feb 2008; accepted 21 Feb 2008; published 11 Apr 2008

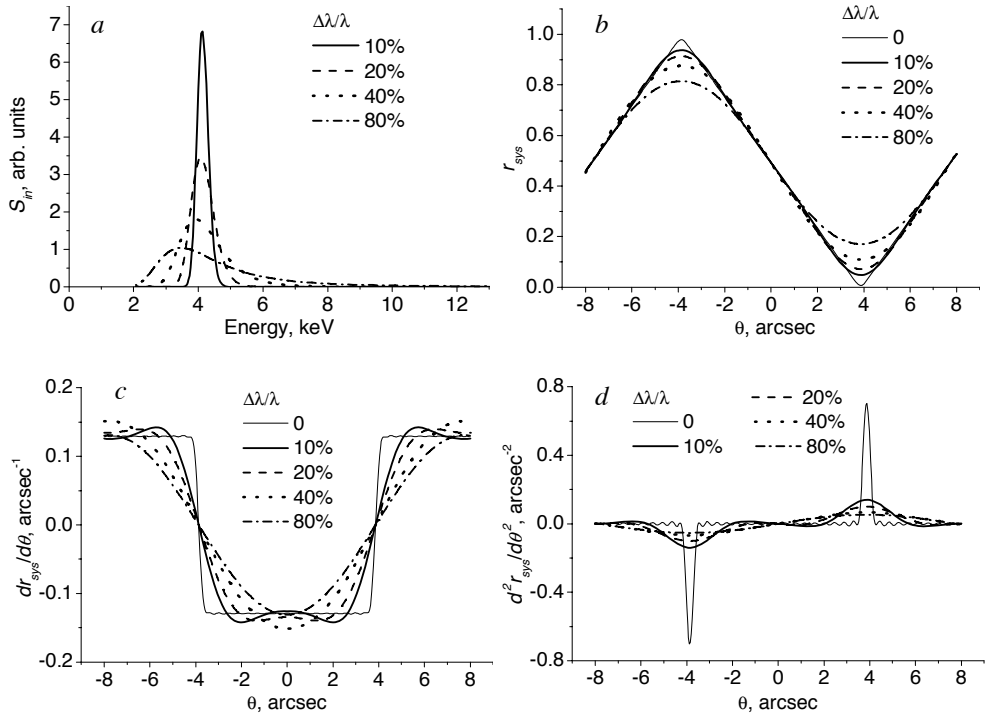

Fig. 4. (a) Model spectral density distributions in X-ray energy (Gaussian distributions with different FWHM, Δλ, were used for λ); (b) simulated 'reflectivity' curves (in the differential contrast regime with $\Delta x = d/4$) corresponding to monochromatic radiation with 3Å wavelength and using the spectra shown in Fig. 4(a); (c) first derivative of the simulated 'reflectivity' curves shown in Fig. 4(b); (d) second derivative of the simulated 'reflectivity' curves shown in Fig. 4(b).

Analysis of the differential contrast images (see Table 4 for details) shows that at least for this particular object and for the generated spectra the differential-contrast images are fairly insensitive to the polychromaticity of the source. Indeed, according to Table 4, the contrast in the image corresponding to 10% spread in the wavelength is only slightly reduced compared to the case of monochromatic incident radiation and the contrast even slightly improves for other spectra shown in Fig.4(a).

By contrast, the dark-field imaging case turned out to be very sensitive to polychromaticity. Analysis of Fig. 5 and Table 4 shows that the contrast in the dark-field images significantly degrades with increasing width of the spectrum (from more than 4% contrast in the monochromatic case down to about 1% contrast in the strongly polychromatic case). At the same time, the background intensity I_{BG} in the dark-field images increases considerably with the increase in the degree of polychromaticity.

Some qualitative explanation of the above behavior of the differential-contrast and dark-field images can be made by analyzing the 'reflectivity' curves of the scanning double-grating imaging system shown in Fig. 4(b). According to this figure, the main effect of polychromaticity on the 'reflectivity' curve is in its smoothing, mostly in the vicinity of its extremes. The geometrical optics approximation (see Section 2.3) predicts that the contrast in the differential-contrast images is proportional to the derivative of the 'reflectivity' in the working point which lies on its slopes. For example, the differential-contrast images have been calculated using the working point positioned in the centre of the negative slope (corresponds to zero deviation angle θ in Fig. 4(b)). Analysis of Fig. 4(c) shows that the magnitude of the 'reflectivity' derivative at this working point remains almost unchanged. On

#92070 - $15.00 USD Received 24 Jan 2008; revised 21 Feb 2008; accepted 21 Feb 2008; published 11 Apr 2008

the other hand, contrast in dark-field images is proportional to the second derivative of the 'reflectivity' curve in the working point positioned at the minima of the 'reflectivity' curve (this corresponds to $\theta \approx 4$ arcsec in Fig. 4(b)-(d)). This second derivative is shown in Fig. 4(d). Analysis of this figure shows that the magnitude of the second derivative monotonically decreases.

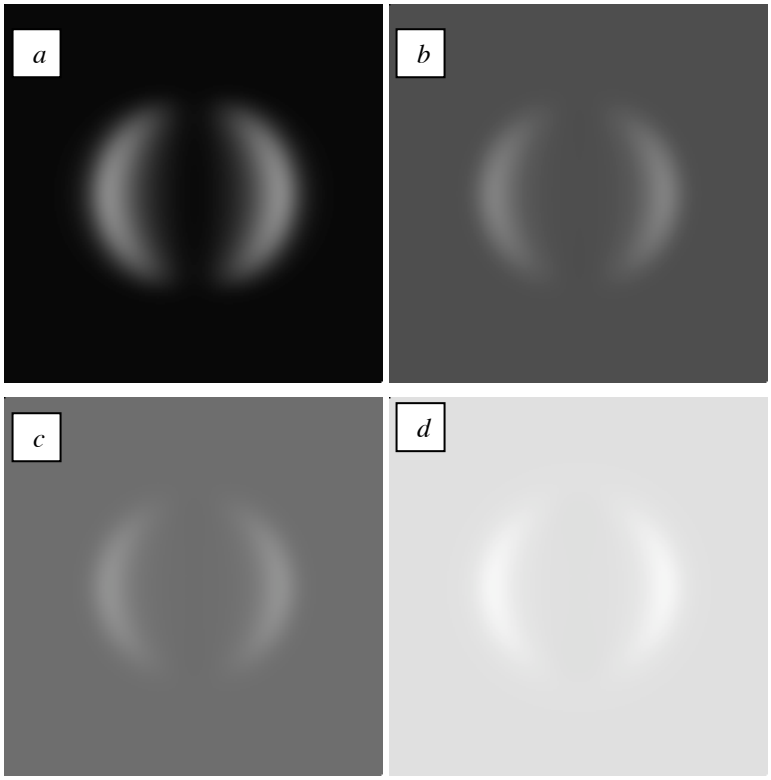

Fig. 5. Dark-field images of a spherical feature of diameter 0.5mm smeared with 100 m (FWHM) Gaussian function, for different values of $\Delta\lambda/\lambda$: 0 (a), 10% (b), 20% (c), 80% (d). The displayed range of intensities in the images is equal to [0, 0.2] (unit intensity of the incident wave is assumed).

5. Conclusion

We have proposed a new grating-based phase-contrast imaging modality in which both gratings are scanned simultaneously while the image is collected and which has significant advantages. In order to evaluate the performance of this new modality, we have derived a rigorous wave-optical formalism describing formation of related images. It should be mentioned that this new formalism can also be successfully applied to the standard (non-scanning) double-grating imaging if both the characteristic size of the features in the object and the detector resolution (often related to pixel size) are sufficiently large compared to the self-imaging period of the first grating. We should also emphasize that the full analysis performed in section 4, including optimization of the instrumental parameters and assessment of the influence of the finite source size and polychromaticity on the image formation, is applicable to any double-grating imaging method (not only to the proposed scanning-double-grating modality).

#92070 - $15.00 USD Received 24 Jan 2008; revised 21 Feb 2008; accepted 21 Feb 2008; published 11 Apr 2008

While the present work is discussed in the terms of electromagnetic radiation in general and X-rays in particular, it is also equally well applicable to the case of phase-contrast imaging using neutrons and to other forms of particles and waves.

#92070 - $15.00 USD Received 24 Jan 2008; revised 21 Feb 2008; accepted 21 Feb 2008; published 11 Apr 2008